



## One year of measurements in Alderney Race: preliminary results from database analysis

Lucille Furgerot, Alexei Sentchev, Pascal Bailly Du Bois, Guillomar Lopez,  
Mehdi Morillon, Emmanuel Poizot, Yann Méar, Anne-Claire Bennis

### ► To cite this version:

Lucille Furgerot, Alexei Sentchev, Pascal Bailly Du Bois, Guillomar Lopez, Mehdi Morillon, et al.. One year of measurements in Alderney Race: preliminary results from database analysis. *Philosophical Transactions of the Royal Society A: Mathematical, Physical and Engineering Sciences*, 2020, New insights on tidal dynamics and tidal energy harvesting in the Alderney Race, 378 (2178), pp.20190625. 10.1098/rsta.2019.0625 . hal-02921140

HAL Id: hal-02921140

<https://hal.science/hal-02921140v1>

Submitted on 26 Aug 2020

**HAL** is a multi-disciplinary open access archive for the deposit and dissemination of scientific research documents, whether they are published or not. The documents may come from teaching and research institutions in France or abroad, or from public or private research centers.

L'archive ouverte pluridisciplinaire **HAL**, est destinée au dépôt et à la diffusion de documents scientifiques de niveau recherche, publiés ou non, émanant des établissements d'enseignement et de recherche français ou étrangers, des laboratoires publics ou privés.

Research



**Cite this article:** Furgerot L, Sentchev A, Bailly du Bois P, Lopez G, Morillon M, Poizot E, Méar Y, Bennis A-C. 2020 One year of measurements in Alderney Race: preliminary results from database analysis. *Phil. Trans. R. Soc. A* **378**: 20190625.  
<http://dx.doi.org/10.1098/rsta.2019.0625>

Accepted: 12 June 2020

One contribution of 14 to a theme issue 'New insights on tidal dynamics and tidal energy harvesting in the Alderney Race'.

**Subject Areas:**

oceanography

**Keywords:**

ADCP, RADAR HF, LIDAR, Alderney Race,  
*in situ* measurements

**Author for correspondence:**

L. Furgerot

e-mail: [l.furgerot@energiedelalune.fr](mailto:l.furgerot@energiedelalune.fr)

# One year of measurements in Alderney Race: preliminary results from database analysis

L. Furgerot<sup>1</sup>, A. Sentchev<sup>2</sup>, P. Bailly du Bois<sup>3</sup>,  
G. Lopez<sup>4</sup>, M. Morillon<sup>3</sup>, E. Poizot<sup>5</sup>, Y. Méar<sup>5</sup> and  
A.-C. Bennis<sup>4</sup>

<sup>1</sup>LUSAC, Laboratoire Universitaire des Sciences Appliquées de Cherbourg, Univ. Normandie, Cherbourg-en-Cotentin, France

<sup>2</sup>Laboratory of Oceanology and Geosciences, Univ. Littoral Côte d'Opale, Univ. Lille, CNRS UMR 8187, Wimereux 62930, France

<sup>3</sup>Laboratoire de Radioécologie de Cherbourg, IRSN-LRC, Rue Max Pol Fouchet B.P. 10, 50130 Cherbourg en Cotentin, France

<sup>4</sup>M2C, Morphodynamique Continentale et Côtière (M2C), Normandie Univ., Caen, France

<sup>5</sup>Intechmer, Conservatoire National des Arts et Métiers, Cherbourg-en-Cotentin, France

LF, 0000-0003-4498-7778; AS, 0000-0001-6971-9505;  
PB-d-B, 0000-0001-8436-0772

The Alderney Race is assumed to have the largest tidal-stream energy potential in the north-western European coastal seas. Interaction of the powerful tidal stream with strong wind, high waves and irregular bathymetry creates hydrodynamic conditions of extreme complexity, with high levels of turbulence. A comprehensive dataset has been created to improve the understanding of physical processes, turbulence, tidal stream and resource variability at the site. The database contains a large amount of oceanographic and meteorological measurements acquired in Alderney Race in 2017–2018. This exceptionally long period of observations (nearly one year) became possible due to modern tools and strategies of data acquisition. The paper presents some significant results from the database analysis. Among many results, we would like to underline the following: (i) a wide range of variability of mean flow and sea state parameters was documented; (ii) exceptionally large values of current velocity

( $7 \text{ m s}^{-1}$ ) and significant wave height (8 m) were measured during extreme meteorological conditions; (iii) high-frequency variability of current speed during storm events was also found to be very large, with the standard deviation of velocity reaching  $0.3 \text{ m s}^{-1}$  in the bottom boundary layer, and  $0.6 \text{ m s}^{-1}$  in the surface layer; and (iv) predominant wind and wave direction relative to the flow impacts the wave height and significantly increases the turbulence kinetic energy of the flow. To our knowledge, this is the largest multi-variable database available on potential tidal energy sites. The results of database analysis can represent a significant advance in environmental conditions and resource characterization and provide advanced information to turbine developers.

This article is part of the theme issue ‘New insights on tidal dynamics and tidal energy harvesting in the Alderney Race’.

## 1. Introduction

Concerns about energy production and climate change are driving transitions towards renewable electricity sources around the world. In recent years, the interest in tidal energy resources has been growing rapidly. Tidal-stream energy has been identified as an energy source with potential as both a renewable and predictable resource (e.g. [1]). The quality of electricity production by tidal energy converters (TECs), close to shore location, good social acceptance level and low environmental impacts make this resource attractive. From 2015 onwards, the first pilot farms, as well as high-capacity single devices, were installed in France (<https://www.sabella.bzh>), the UK (e.g. [2]; <https://simecatlantis.com>) and the Netherlands (<https://www.tocardo.com>). Faced with this increase in capacity, the need for research has also grown.<sup>1</sup>

The first step in a long chain of development of the tidal-stream industry, from resource assessment to device design and operation, requires characterization of the flow environment at a variety of spatial and temporal scales at potential sites. Coastal flow characterization for tidal-stream applications relies on the measurement of current velocity at large spatial scale given the non-uniformity of the flow field. Therefore, no single instrument measurements but multi-instrument and multi-parameter measurements are required by the sector in order to acquire the necessary data inputs. Development of a local observing system for monitoring coastal flow, sea state, atmospheric conditions for marine industrial or environmental applications is difficult and expensive (e.g. [3]). Environmental constraints (e.g. large flow speed, short time window suitable for instrument deployment and recovery, complex bathymetry, favourable weather conditions, etc), in conjunction with technical constraints, often limit the period of observations to 1–2 months [4–6].

Characterization of current, wave and turbulence—and the interaction between these processes—are used to predict available resources (e.g. [7,8]), to determine power quality fluctuations [1] and to assess fatigue and extreme loading of TECs (e.g. [9]). Required both for individual TECs and arrays of TECs, an accurate description of a highly energetic and highly turbulent tidal flow helps engineers to improve the performance of TECs (e.g. [10,11]). This contributes to the reliable and predictable production of grid quality power at costs competitive with other forms of energy generation [12].

Moreover, the data acquired by a network of instruments helps to improve numerical models which are extensively used for assessing the tidal-stream resource variability at larger temporal and spatial scales.

This paper presents a large database of oceanographic and meteorological measurements acquired in 2017–2018 at a potential tidal-stream energy site in the eastern sector of Alderney Race—in French territorial waters. The site, located between the Cotentin Peninsula (France) and Alderney Island (a British Crown dependency), is considered to have the largest potential in

<sup>1</sup>Information in this paragraph sourced from web searches.

north-western Europe. According to a numerical study by Coles *et al.* [13], the maximum power that can be extracted in this shallow water 15 km-wide strait, is estimated at 5.1 GW, which is 35% more than a previous estimate proposed by Draper *et al.* [14] for the Pentland Firth (UK). The complexity of local hydrodynamics and the interaction between the highly irregular bottom topography [15], powerful tidal stream and high waves was highlighted in a number of numerical studies devoted to this geographic area (e.g. [16–18]). This was also supported by an observation-based study [6]. All these studies covered relatively short time periods (less than one month) or were focused on specific (storm) events.

However, even if tides are considered predictable due to their regular periodicity, the persistence and variability of tidal stream in the Alderney Race, in conjunction with large wave–wind forcing, is unknown. This paper is the first study that attempts to address this knowledge gap through direct measurements.

Modern tools for observation of tidal hydrodynamics, wave motions and wind–wave–current interaction were developed and applied in the Alderney Race. These include, for instance, remote sensing of currents and waves with high spatial and temporal resolution by high-frequency radars, underway velocity measurements by towed ADCP systems, long-term (one-year long) static point measurements of current velocity and waves, wind speed profiling by atmospheric LIDAR, etc. The methodologies used in data analysis were also diversified.

As the tidal flow in the Alderney Race is often affected by high waves and winds, the quantity of data which have been acquired during ‘calm periods’ is not large. We preferred these ‘calm periods’ for assessing small scale variability of current velocities, affected by bottom friction-generated turbulence. Conversely, wave and wind forcing and their interaction with currents were on the basis of other periods of observations. These also include storm events with resulting sea state characteristics that were never documented before. Wave and wind measurements at buoys/anemometers located outside of the Alderney Race were included in the database and found to be useful for a better understanding of the variability of currents.

Spatial variability of tidal stream was assessed by using underway velocity measurements by towed ADCP and remote sensing of surface currents by HF radars. These techniques were employed only recently for tidal-stream resource characterization at prospective sites (e.g. [7,19–21]). We present below a detailed description of the database and some results from the database analysis.

## 2. Data and methods of analysis

### (a) Static point velocity measurements by bottom-mounted ADCP

A total of seven oceanographic campaigns were performed in the Alderney Race from April 2017 to July 2018. All campaigns targeted neap tide conditions suitable for deployment, recovery and quick redeployment of ADCPs on the seafloor. This strategy allowed us to acquire long time series of current velocities.

Three bottom-mounted ADCPs, approximately 1.5 km apart and referred to hereafter as S1, S2, S3, were aligned in the east–west direction in the south-eastern sector of the Alderney Race, in French territorial waters (figure 1a). Figure 1a also shows the maximum tidal current speed in the Alderney Race from numerical simulations by the high-resolution two-dimensional model of Bailly du Bois *et al.* [23]. Initially, the deployment of ADCPs was expected a few kilometres northward where the tidal stream is more energetic. However, two conditions obliged us to change the location. A preliminary study revealed that, in the northern sector, the seafloor is mostly composed of Proterozoic crystalline rocks that exhibit a dense fracture network and form a highly irregular topography [15]. Therefore, our ADCP support platforms were thought to be more unstable there. The second condition was related to the strength of the tidal stream which, in combination with the large occurrence of high waves, made the schedule of deployment impossible to keep. For example, the recovery of the northern ADCP (S4), installed by divers on the seafloor in September 2017 was delayed by four months. This ADCP performed the data

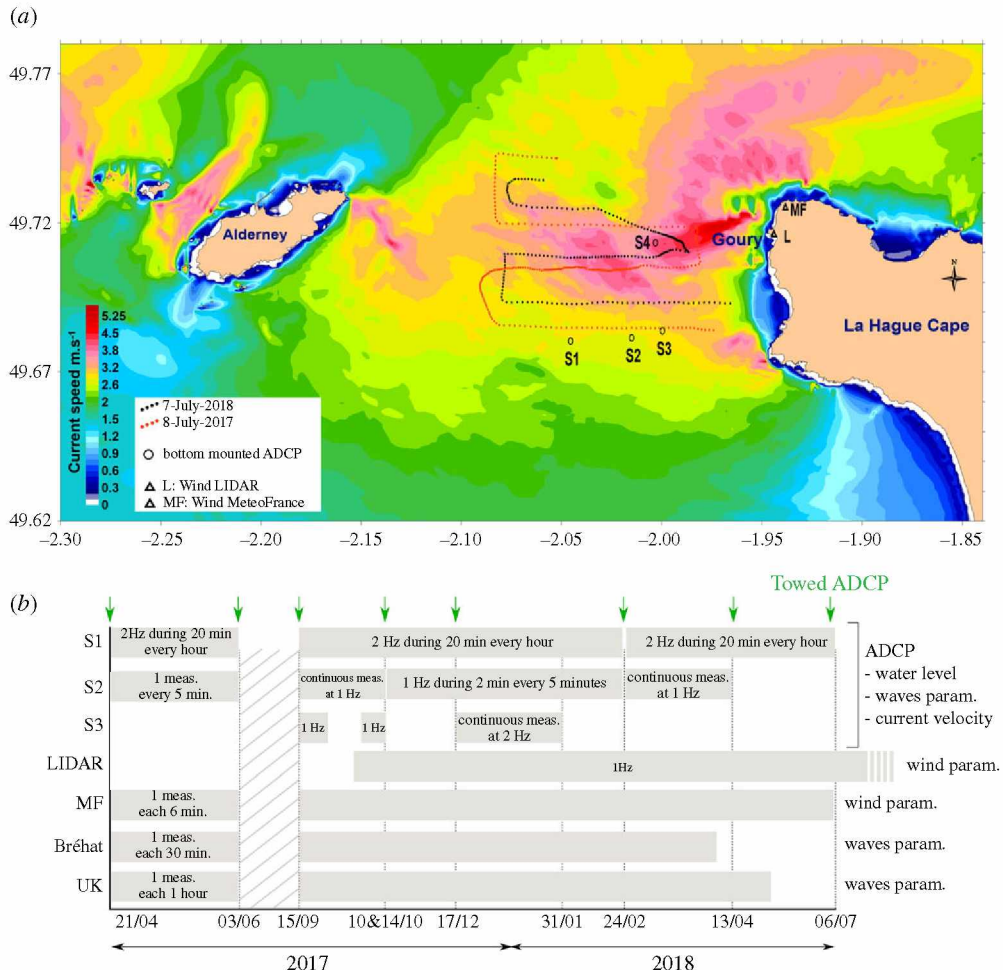


**Figure 1.** (a) Location of the study site and the instruments performing data acquisition in the Alderney Race in 2017–2018. ADCP locations S1–S4 are shown by circles. Towed ADCP survey transects in July 2018 are shown by red and blue dots. Atmospheric LIDAR (L) and MeteoFrance (MF) meteorological station locations are shown by triangles. Background shading represents the maximum current speed flood from numerical simulations by regional model MARS-2D (e.g. [22]). (b) Summary of the measurement setup and periods of data acquisition in the Alderney Race from 21 April 2017 to 6 July 2018. Green arrows show the oceanographic campaigns devoted to the deployment of ADCPs on the seafloor and towed ADCP surveys. (Online version in colour.)

acquisition during 38 days and was not used again. The detailed analysis of S4 ADCP data are given in [6,21] and in the present Theme Issue. Therefore, three ADCPs were deployed in a less energetic area where Quaternary cobbles and blocks form a relatively flat seafloor. Although all experimental platforms have been designed to resist strong currents, high pressure and impacts by moving pebbles or small rocks, some technical problems and failures were encountered: (i) five ADCPs suffered from water infiltration; (ii) one ADCP was lost; (iii) the acoustic release devices sometimes failed or were delayed, thus preventing the platform being recovered during several days (duration of a survey); and (iv) rough meteorological conditions making the oceanographic campaigns difficult or shorter than initially expected. Nevertheless, a large quantity of data has been acquired representing an extensive database which contains 334 days of data (almost continuous time series) with only one prolonged break during summer 2017. Figure 1b provides the time history of ADCP deployment and the data acquisition strategy.

Two versions of RDI-Teledyne upward looking ADCPs were used: a 500 kHz five-beam ADCP-Sentinel V50 (in location S1 and S3) and a 600 kHz four-beam ADCP Workhorse Sentinel (in location S2). The cell size was set to 1 m for each instrument and the first bin was located 2 m above the base of the platform, installed motionlessly on the seafloor. S1 ADCP (V50) was configured to perform simultaneous velocity profiling and wave measurement over 20 min every hour (2 Hz burst mode), and one measurement per second (1 Hz) over one minute, repeated every five minutes (Table figure 1b). The configuration of ADCP S2 and S3 evolved during different deployment periods, with respect to autonomy of batteries and memory capacity (figure 1b). The velocity data were recorded in the ENU coordinate system and checked for the quality of the signal: the data with correlation lower than 90 and with amplitude lower than 75 counts were removed, following the method proposed by Kirincich & Rosman [24]. Then the despiking filter of Goring & Nikora [25] was applied. During the second step, the data contaminated by the acoustic signal reflection from the sea surface were removed. Such an interference zone strictly depends on the angles between the ADCP beams. This angle measures 25° for the ADCP-V50 and 20° for the ADCP Workhorse600 kHz, thus corresponding to a fraction of the water column affected by contamination of the order of 11% and 6%, respectively [26].

The horizontal velocity magnitude  $\bar{U}_{\text{mag}}$  and direction were estimated at different depth levels from ENU velocities for 20 min averaging intervals every hour during the whole period of observations. The turbulence kinetic energy (TKE) and the standard deviation (std) of velocities around the 20 min mean velocity were also estimated to characterize the flow variability. These parameters provide a quantification of turbulent fluctuations which are considered to be dominant drivers of the fatigue loads on tidal turbine blades [27].

Parameters of waves, wind and tidal stage (neap/spring/flood/ebb tide) were associated with each 20 min averaged velocity value. This allowed us to create a complete database of the environmental conditions over a one-year period and can be sorted according to current intensity, significant wave height or wind intensity.

## (b) Wave and wind measurements

The major parameters characterizing the sea state in the Alderney Race were assessed using Sentinel V50 ADCP and high-frequency (HF) radars (results of wave measurements by HF radars are not presented in this paper).

Wave parameters from ADCP were calculated using WavesMon RDI software that employs the orbital velocity method for estimating significant wave height ( $H_s$ ), peak period ( $T_p$ ) and the provenance direction of waves—main peak direction ( $D_p$ ). Each sample contained 2400 measurements (20 min burst). FFT was applied to 2048-long samples with three averaging intervals of 6 min each, as recommended in the manual of WaveMon software [28] available on the website of Teledyne. This time interval is a good compromise allowing us to take into account the high variability of tidal flow and the noise reduction by averaging. According to Wiberg and Sherwood [29], the orbital velocity method is assumed to be reliable, especially when the spectral analyses of the sea surface variations cannot be done. This is the case in our study as the pressure sensor of ADCP did not work most of the time.

Two wave buoys located close to the study area were used to more broadly assess the sea state variability in the western English Channel and to validate the results derived from ADCP measurements. One buoy is located 20 km north of the Brehat Island and 96 km southwest of Alderney Race (buoy of Candhis network). Another buoy (buoy 62103 of the UK Met Office network) is located 70 km northwest of Alderney Race. The data from buoy measurements include  $H_s$ ,  $T_p$ , and  $D_p$  (only for the Bréhat buoy). Buoy 62103 of the UK Met Office is non-directional.

In this paper, parameters of the sea state derived from measurements by different devices are compared and then, global statistics are provided for  $H_s$ : the occurrence diagram and wave roses.

Wind measurements in the study area were performed at a meteorological station, MétéoFrance station (MF), located at the semaphore of Goury (figure 1a). Wind speed and direction were measured at 10 m above the ground level (AGL). This altitude is a reference in

all wind studies. Parameters were averaged within 6 min (with a 10° precision for the direction). To complete this point measurements, vertical profiles of wind were recorded by Windcube LIDAR, also installed at Goury (1.3 km south of the meteorological station) from 10/10/2017 to 15/01/2019. The profiles were acquired at 1 Hz in the layer extending from 40 to 290 m AGL. These measurements are distant from S2 ADCP location by 8.3 and 7 km, respectively.

### (c) Towed ADCP measurements and optimal interpolation of velocities

A total of six towed ADCP surveys were carried out in the Alderney Race during the campaigns devoted to the deployment and recovery of bottom-mounted ADCPs (green arrows in figure 1b). Only results of two longest surveys will be presented below. They were also selected for their largest spatial coverage and velocity profiling in the whole water column. The flood tide survey lasted 4.5 h (11:15–15:40 UTC) on July 7, 2018, and the ebb tide survey also lasted 4.5 h (06:30–10:50 UTC) on July 8, 2018. The weather conditions were good: the wind speed less than  $4 \text{ m.s}^{-1}$  and waves less than 0.5 m. Underway velocity measurements were performed by using two experimental platforms deployed simultaneously: one—a subsurface platform, carrying a broadband ADCP (600 kHz Teledyne WorkHorse Sentinel), and another—a surface platform, carrying a 1.2 MHz Teledyne ADCP. Both platforms were towed by the R/V 'Côtes de la Manche'.

The first deep-towed depressor platform 'Dynalest' was developed at the National Institute for Radioprotection and Nuclear Safety (IRSN) for operating an in-depth sampling system while the vessel moves at a speed up to  $5 \text{ m s}^{-1}$ . During the surveys, the platform was located roughly 7 m below the water surface to avoid perturbations by the wake. More details about the Dynalest design and application can be found in [30]. The second experimental platform 'Koursk' was towed on the surface and carried a surface mounted ADCP. The distance from the boat central axis was controlled by an adjustable side fin allowing it to avoid contamination by the wake of the boat. The ADCP's transducer head was located 0.3 m below the water surface and the centre of the first bin was roughly at 1 m depth. Current velocities recorded by ADCPs were corrected for vessel motion and averaged within 1 min intervals. GPS coordinates were also sub-sampled every minute, so that the distance between the thinned along-track data points varied within 120–180 m, depending on the towing speed. Velocity profiles derived from two instruments, overlapping within 8–15 m depth layer, were merged and the resulting profiles, at 1 min spacing, extended from surface (starting 1 m below the sea surface) to near bottom.

Towed ADCP measurements from repeated transects contain information on both spatial and temporal variations of tidal currents and a number of techniques have been used to separate these variations. Some of them use harmonic representation of velocity evolution. This approach brings artificial disturbances into the spatial structure of the velocity field while methods based on biharmonic splines impose spatial smoothness on the interpolated field, which is a reasonable choice for many applications where temporal variability could be neglected [31]. More recently, Goddijn-Murphy *et al.* [19] used a numerical model for velocity interpolation in the Orkney straits (Pentland Firth). Their approach aimed to preserve the dynamically consistent structure of the flow (i.e. the physics of tidal motions).

A straightforward way of statistically consistent interpolation of a vector field is the well-known method of optimal interpolation (OI) pioneered by Gandin [32] and, since then, widely adopted in geosciences (e.g. [33,34]). Sentchev & Yaremchuk [35] employed the OI technique by including the time dimension and used the space–time correlation functions derived from numerical model simulations. The authors reconstructed the evolution of tidal current velocity field in the Boulogne harbor (English Channel) by interpolating the velocity measurements by towed ADCP and obtained a considerable improvement compared to pure model simulations.

The same approach was used to process the velocity measurements acquired in the Alderney Race during the towed ADCP surveys in July 2018. In this approach, the optimal correction to the evolution of a background velocity field on a regular (model) grid is represented by a linear combination of the weighted differences between the background model trajectory and the observed velocities. The weights are chosen to minimize the mean square difference between the

observations and the background (model) velocities. As the result, OI provides a set of snapshots of the velocity vector field on a regular space–time grid for the entire period of observations, with time resolution defined by the user. The regional model MARS-2D, configured for high-resolution simulations in the surveyed area [23], was used to generate the background velocities and the space–time correlation functions. More technical details on the application of the OI technique can be found in [35] and references therein.

#### (d) Current mapping by high-frequency radars

An innovative approach to assessing the space–time variability of circulation in the Alderney Race is based on the use of remote sensing of surface currents. Two HF Wellen Radars (WERA), operating at frequencies 13.5 and 24.5 MHz, have been deployed on the northwest coast of the Cotentin peninsula since the beginning of 2018. Individual radar sites are located at Cape Jobourg and at Goury (figure 1a). The distance between sites is approximately 5 km which is not favourable for current mapping at far ranges but sufficient to get a complete coverage of the Alderney Race. The radars measure the current velocity in the surface layer of a thickness which is proportional to the radio wavelength  $\lambda_R$ . The effective depth of velocity measurements by the radar, determined as  $\lambda_R/8\pi$  [36], is equal to 1 m and 0.5 m, respectively, for two radio wavelengths,  $\lambda_R = 22.2$  m and  $\lambda_R = 12.2$  m, used in the Alderney Race by the radars operating at two frequencies.

The recorded radial velocities are the projections of the current velocity vector onto radar beam directions. Two radar network configurations have been used for retrieving radial velocities of surface currents: a high spatial resolution configuration with 0.75 km along the beam and 3° azimuthal spacing, and a low resolution configuration with 1.5 km along the beam and 7° azimuthal spacing. Temporal resolution was set to 30 min.

The standard technique of the phased array radar data processing involves the use of the beam forming (BF) method (e.g. [37]) which provides the azimuthal resolution of 7°. To obtain higher (3°) resolution radial velocity maps, the HFR signals were reprocessed by using the Multiple Signal Classification (MUSIC) direction finding (DF) algorithm of Schmidt, [38] driven by the parameterization of Lipa *et al.* [39]. The maximum value of radial velocity measured by a radar operating at a wavelength  $\lambda$  (13.5 MHz) is limited by  $f_B \cdot = \lambda/2$  ( $4.4 \text{ m s}^{-1}$ ), where  $f_B$  is the Bragg frequency corresponding to the radar frequency. However, the DF method was found to be noisy. Thus, techniques of noise removal, despiking and gap filling were applied to remotely sensed data before reconstructing the radial velocity time series. The detailed description of the radar network configuration and methods of data processing can be found in [40,41].

Radial velocities measured by two radars were interpolated on a regular grid of 1 km spacing and combined to form current vectors using the variational interpolation technique—2dVar [42]. This technique provides an efficient control of smoothness, divergence and vorticity of the resulting velocity vector maps. The size and shape of the interpolating area was chosen so as to ensure reasonably low values of errors due to geometric dilution of precision (GDOP), i.e. the minimum angle of beam cross-section was less than 20° everywhere within the area.

### 3. Preliminary results of data

#### (a) Time variability of meteorological and hydrodynamic conditions

Meteorological and hydrodynamic conditions revealed large variations during the period of measurements. As expected, an important distinction is observed between the summer and winter periods (figure 2). The summer period was characterized by calm weather and relatively low waves on average (from the end of April to October), while several storms occurred in winter generating  $H_s$  up to 8 m (figure 2). Storm events encountered during the measurement period were associated with strong persistent winds and correspond to high waves events.

A good correspondence was observed between the wind measurements by LIDAR (the first cell of measurements) and that at the MF station (figure 3a), with correlation  $R^2 = 0.93$  despite

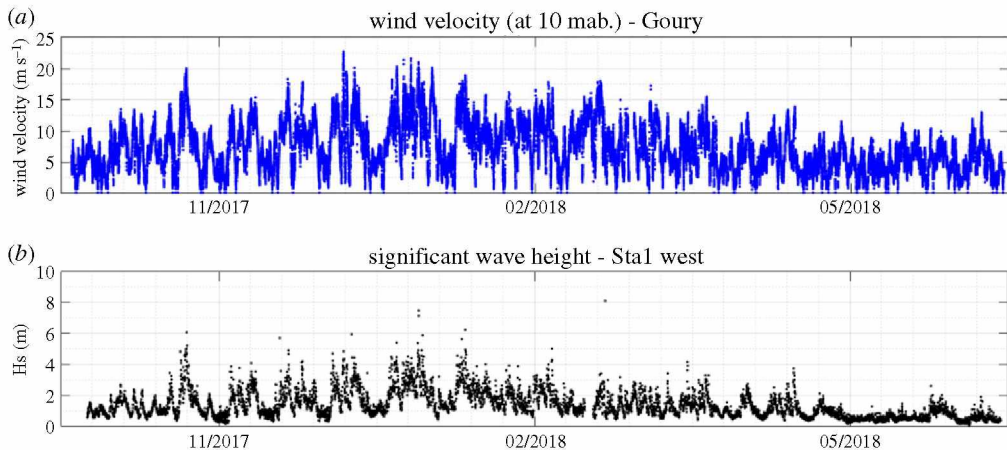


**Figure 2.** Time series of wind measurements at Goury MF station (a) and  $H_s$  measurements at S1 ADCP location (b). (Online version in colour.)

the difference in measurement height (40 m AGL versus 10 m AGL). The wind speed at 40 m AGL was found to be larger than at 10 m AGL in accordance with the logarithmic shape of the velocity profile. Wind speed at Goury (10 m AGL) shows a range of variations from 0 to 23  $\text{m s}^{-1}$  with values larger than 6.5  $\text{m s}^{-1}$  observed half of the time (figure 3b). The area is considered as very windy. Low wind (speed less than 4  $\text{m s}^{-1}$ ) was observed 23% of the time, while storm conditions, with wind speed exceeding 15  $\text{m s}^{-1}$ , occurred 2.5% of the time. The area is affected by two dominant wind directions with wind blowing from the southwest sector ( $180^\circ$ – $270^\circ$  with respect to the north) 38% of the time and from the east sector 15% of the time ( $70^\circ$ – $95^\circ$ ) (figure 3c).

Significant wave height and directions derived from ADCP and two wave buoys measurements were compared (figure 4a,b) for evaluating the quality of the ADCP data. Since the three measurement points are far apart, it is difficult to directly compare the respective wave parameters because of the delay induced by wave propagation in each area. Qualitatively, storm events recorded by the three stations are in phase in time (green arrows in figure 4a). On average, over the whole year,  $H_s$  estimated from the ADCP are lower than that estimated at Bréhat (42 cm lower) and by buoy 62103 (20 cm lower) probably related to the distance between measurement points (difference in bathymetry, general morphology, approach of the waves to the coast, presence of Alderney Island).

Wave directions at Bréhat buoy location show that this near shore area is dominated by waves arriving from the west and west-north-west sectors (figure 4b). These waves come from the Atlantic Ocean with a significant contribution of fetch with large wavelength. In the Alderney Race, the observed waves are characterized by larger dispersal of directions (from  $240^\circ$  to  $300^\circ$  with respect to the north) which is related to the exposure of the Race to long swell from the Atlantic Ocean. The period of these waves can be very long (up to 18 s) as shown on figure 4d. Another statistically significant direction of waves is from the north (approx. 10% of cases in figure 5). These waves, originating from the eastern part of the English Channel, are propagating westward and refracted by the La Hague Cape. They are characterized by low  $H_s$  and  $T_p$  lower than 8 s (figure 4d).

The average  $H_s$  is 1.3 m in the Alderney Race and the most common  $H_s$  is between 0.4 and 1 m (figure 4c). Waves with  $H_s$  lower than 0.5 m were observed 13.5% of the time and extreme events with  $H_s$  larger than 4 m occurred 1.2% of the time. Analysis of the wave data at Brehat for the same period shows that 4% of the time,  $H_s$  was greater than 4 m and 6.2% of the time, it was lower than 0.5 m. All of these events come from the west with  $T_s$  between 10 and 16 s.

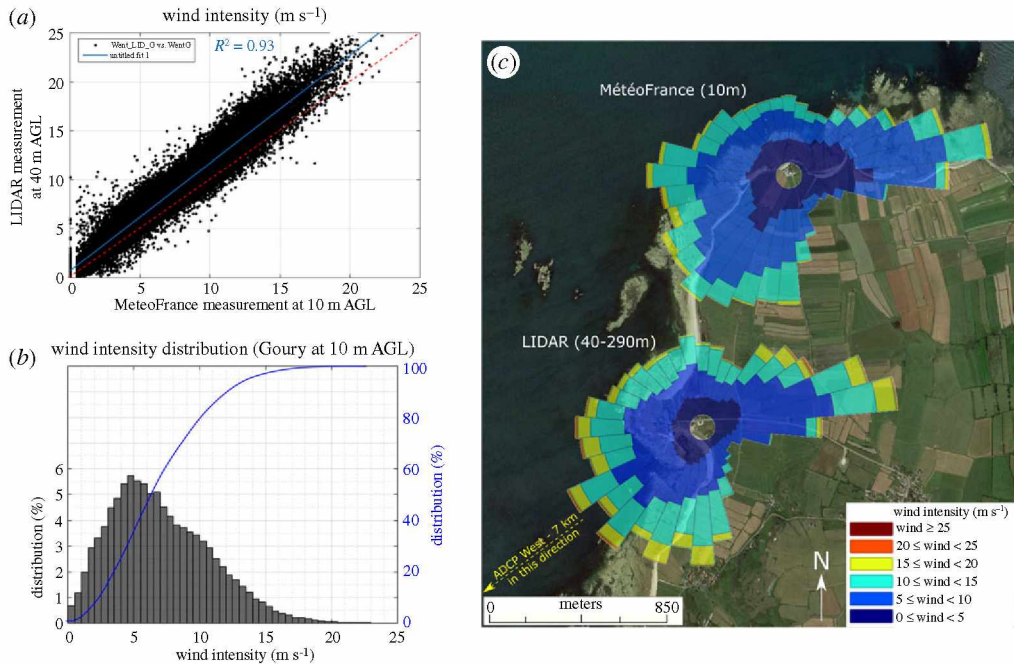


**Figure 3.** (a) Comparison of wind intensity ( $\text{m s}^{-1}$ ) between Goury meteorological station (10 m AGL—Above ground level) and first cell of lidar (40 m AGL) (location on map C); (b) Distribution of wind intensity in Goury MF station; C. Wind rose for MF station and Lidar station (40 m AGL) with colour shading shows in addition to origin, the occurrence of wind intensity (in relative %). (Online version in colour.)

Seven major storms can be identified in the time series of ADCP measurement in January 2018 (figure 4a) with  $H_s$  higher than 4 m, and one exceptional event in January 2018 ( $H_s = 8$  m) during the Eleanor storm, shown by the second green arrow in figure 4a. This event is recorded by all buoys (Bréhat and 62103 buoy) with similar  $H_s$  values and a peak period of 12–13 s.

## (b) Flow variability: from tidal period to high-frequency scale

### (i) Averaged variability

Tidal motions with semi-diurnal period dominate the flow variability in the Alderney Race and in the English Channel. With tidal range varying from 1.8 to 7.8 m in the database, the flow regime can be qualified as hypertidal, following the classification of Archer [43]. The dynamics of the associated tidal currents is an example of a progressive wave system. The largest velocities were therefore observed during the high water and low water while the weakest current occurred at mid-time of rising and falling tide (figure 5a). All three ADCP measurements revealed the same variability of currents. On average, in the whole water column, the 5 min averaged current speed at three locations are very similar with correlation  $R^2 = 0.96$  and  $R^2 = 0.97$  for S2/S3 and S1/S2 ADCP, respectively (figure 5b).

The maximum depth averaged current speed was found to be  $3.0 \text{ m s}^{-1}$  during high tide and  $2.6 \text{ m s}^{-1}$  during low tide in all three ADCP locations (S1, S2 and S3). Larger current speed ( $4 \text{ m s}^{-1}$ ) was recorded in the surface layer, again in three locations. Velocity fluctuations, instantaneously measured at 2 Hz, can reach  $7 \text{ m s}^{-1}$  under strong wind and wave forcing. The maximum depth averaged velocity was found to be larger in the northern sector of the Alderney Race, at location S4 (figure 1a). The current speed both on flood and ebb tide reached  $5 \text{ m s}^{-1}$  there during spring tide conditions.

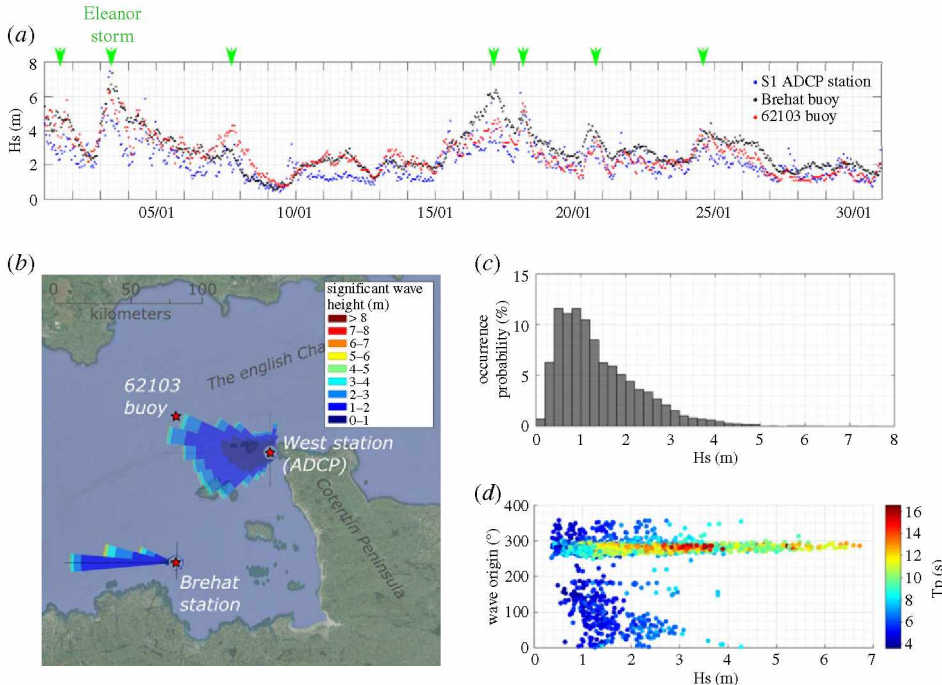


**Figure 4.** (a) Comparison of significant wave heights from wave buoy measurements and ADCP-S1: Buoy of Brehat (Candhis network), buoy 62103 (UK Met Office network) and ADCP-V50 (S1) on January 1–January 31, 2018 (storms indicated with green arrows); (b) Wave measurements location: Bréhat buoy, buoy 62103 (non-directional buoy), and ADCP-S1. Wave roses with colour shading shows the occurrence of  $H_s$  (in relative %); (c) Histogram of  $H_s$  calculated from the ADCP-S1; (d) Scatterplot of  $T_p$  and  $H_s$  with respect to wave direction (Origin) derived from ADCP-S1. (Online version in colour.)

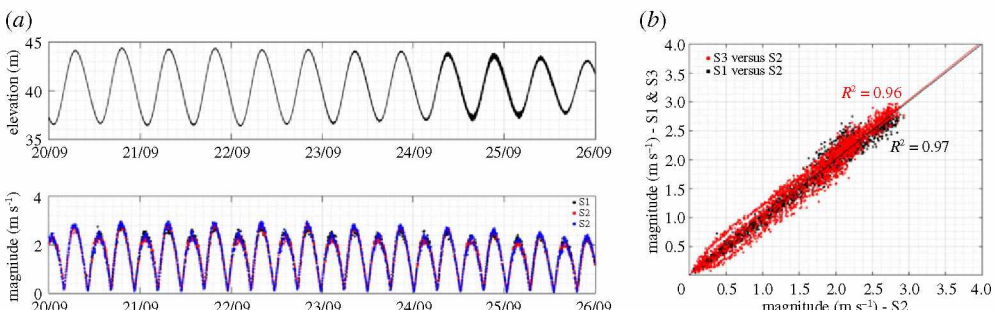


**Figure 5.** Comparison of 5 min averaged and depth averaged current speed recorded by three ADCPs (period used in comparison spans from 20/09 to 26/09 2017). (a) Evolution of the water level and current magnitude in S1, S2 and S3. (b) correlation between S3 and S2 ADCP measurements (red points) and S1 and S2 ADCP measurements (black points). (Online version in colour.)

The tidal flow is nearly rectilinear with flood directed toward NNE ( $20^\circ$ ) and ebb toward SSW ( $190^\circ$ ) (S1 and S2 ADCP—figure 6). The tidal current ellipse is characterized by low ellipticity value (approx. 0.05) and current vector rotates counterclockwise.

Figure 5a and figure 6 indicate a tidal current velocity asymmetry with flood-tide dominant regime in all three ADCP locations. For example, the maximum velocity during the flood of September 21 is  $3\text{ m s}^{-1}$ , while it is  $2.5$  and  $2.6\text{ m s}^{-1}$  during the adjacent ebb phases (figure 5a).

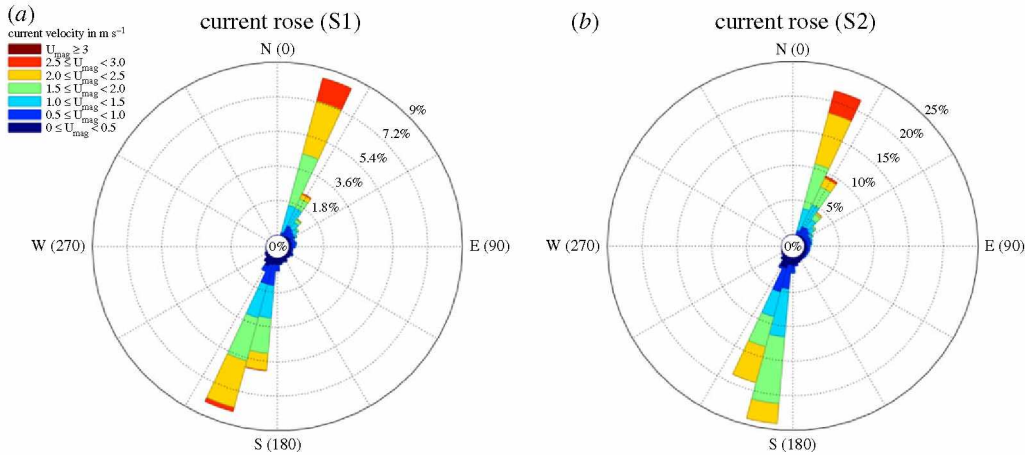


**Figure 6.** Rose of current direction and current speed (colour shading) at S1 (a) and S2 (b) ADCP locations. (Online version in colour.)

## (ii) High-frequency variability of velocity

Velocity fluctuations were assessed for calm weather conditions characterized by  $H_s$  less than  $0.5 \text{ m}$  and wind speed less than  $4 \text{ m s}^{-1}$ . These conditions were observed only 6% of the time, during which the impact of wind and waves on tidal currents is assumed to be negligible. Two 20 min periods were chosen to illustrate qualitatively the current speed variability for two contrasting flood flow conditions: low flow velocity (LV:  $0.5 \text{ m s}^{-1}$ ) and high flow velocity (HV:  $2.5 \text{ m s}^{-1}$ ) (figure 7). For LV, the range of velocity variability around the mean was close to  $0.2 \text{ m s}^{-1}$  at all depth levels. For HV, the velocity varied in a much wider range: from  $1 \text{ m s}^{-1}$  to  $3 \text{ m s}^{-1}$ . The velocity shear can reach large values during certain times. For example, at time 18 min in figure 7, the velocity is close to  $1 \text{ m s}^{-1}$  at 2 m above the bottom, while it is  $3 \text{ m s}^{-1}$  at 30 m above the bottom. The resulting mean shear is  $0.07 \text{ m}^2 \text{s}^{-2}$ , which is typically observed only in the bottom boundary layer where the flow experiences friction from the seabed. This example and velocity time series shown in figure 7 shed light on a large effect of the bottom friction and turbulence capable of generating highly sheared velocity profiles.

TKE is a quantity suitable for assessing the velocity fluctuations within 20 min periods. Evolution of TKE at two depth layers for all periods without waves is shown in figure 8. Vertical profiles of the standard deviation of current velocity for the same periods are shown in red in figure 9. TKE was estimated from velocity time series recorded by S1-ADCP in the measuring cell closest to the bottom (approx. 2 m) and in the cells corresponding to a height of 85% of the water column taking into account the sea surface tidal variability (figure 8). A non-linear increase of TKE with respect to current speed is observed in the bottom layer while the values of TKE in the surface layer remain constant. In the surface layer, the level of ambient turbulence is 5 times lower ( $\text{TKE} = 0.02 \text{ m}^2 \text{s}^{-2}$ ) than in the bottom layer ( $\text{TKE} = 0.1 \text{ m}^2 \text{s}^{-2}$ ). Close to the surface, a weak modulation of turbulence by the tidal phase is observed only for high speeds (greater than  $1.5 \text{ m s}^{-1}$ ) with a higher level of TKE found on ebb flow ( $0.03 \text{ m}^2 \text{s}^{-2}$ ) than on flood flow ( $0.02 \text{ m}^2 \text{s}^{-2}$ ). In the bottom layer, the time evolution of TKE follows different laws and depends on the tidal stage (flood, ebb tide and slack water), with a much larger level of turbulence (up to  $0.16 \text{ m}^2 \text{s}^{-2}$ ) found on ebb flow, compared to  $0.12 \text{ m}^2 \text{s}^{-2}$  on flood flow.

Vertical profiles of standard deviation for  $H_s < 0.5 \text{ m}$  (red curves figure 9) reveal also that the largest variability of current velocities occurs near the seafloor. This variability considerably increases (by the factor of 3: from 0.1 up to  $0.3 \text{ m s}^{-1}$ ) while the flow speed increases from  $0.5$  to  $2.6 \text{ m s}^{-1}$ , thus evidencing a high level of turbulence generated by bottom friction at large current velocity.

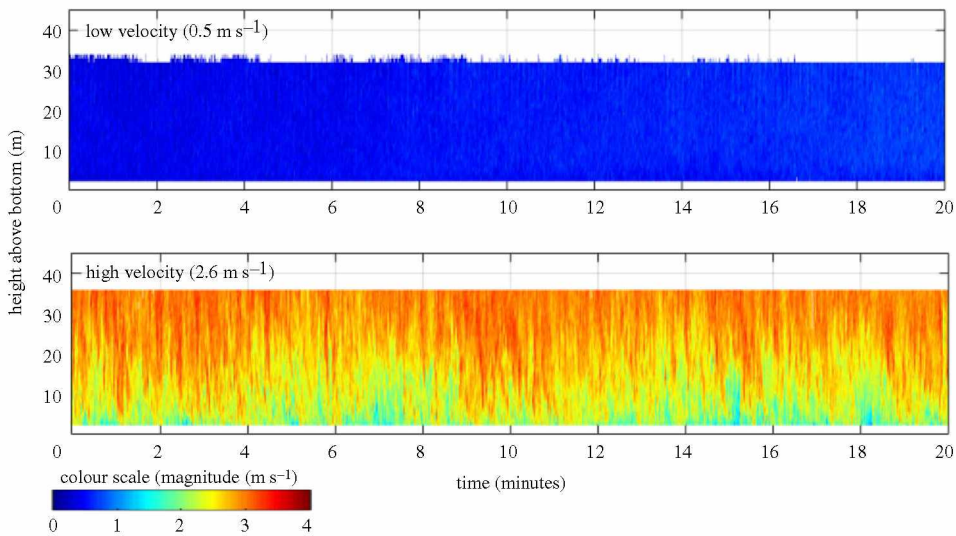


**Figure 7.** Variability of the flow speed (colour shading) during 20 min of measurements (one burst) by S1-ADCP for calm weather conditions ( $H_s < 0.5 \text{ m}$ , wind speed less than  $4 \text{ m s}^{-1}$ ) and for two contrasted flow regimes: with low mean velocity ( $0.5 \text{ m s}^{-1}$ ) and large mean velocity ( $2.6 \text{ m s}^{-1}$ ). (Online version in colour.)

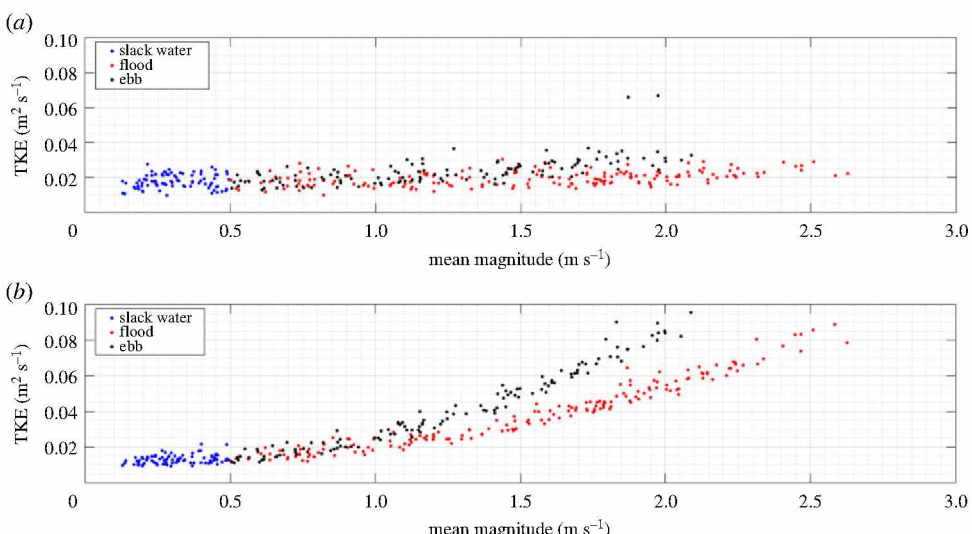


**Figure 8.** Turbulence kinetic energy in the (a; 2 m above bottom) and in the (b) of the water column (85% of the water column height) during all 20 min intervals of time corresponding to calm weather conditions ( $H_s < 0.5 \text{ m}$  and wind speed less than  $4 \text{ m s}^{-1}$ ). (Online version in colour.)

The bottom friction affects the tidal current and modifies the velocity profile shape, making the profile more sheared. The velocity shear in turn contributes to turbulent energy production and its propagation toward the upper layers. Red curves in figure 9 reveal that nearly half of the water column, extending up to 15 m above the bottom, is strongly affected by turbulent motions (standard deviation is multiplied by two from  $0.12 \text{ m s}^{-1}$  to  $0.25 \text{ m s}^{-1}$ ). On the contrary, in the surface layer, the level of ambient turbulence is the same ( $0.12 \text{ m s}^{-1}$ ) regardless of the average speed value.

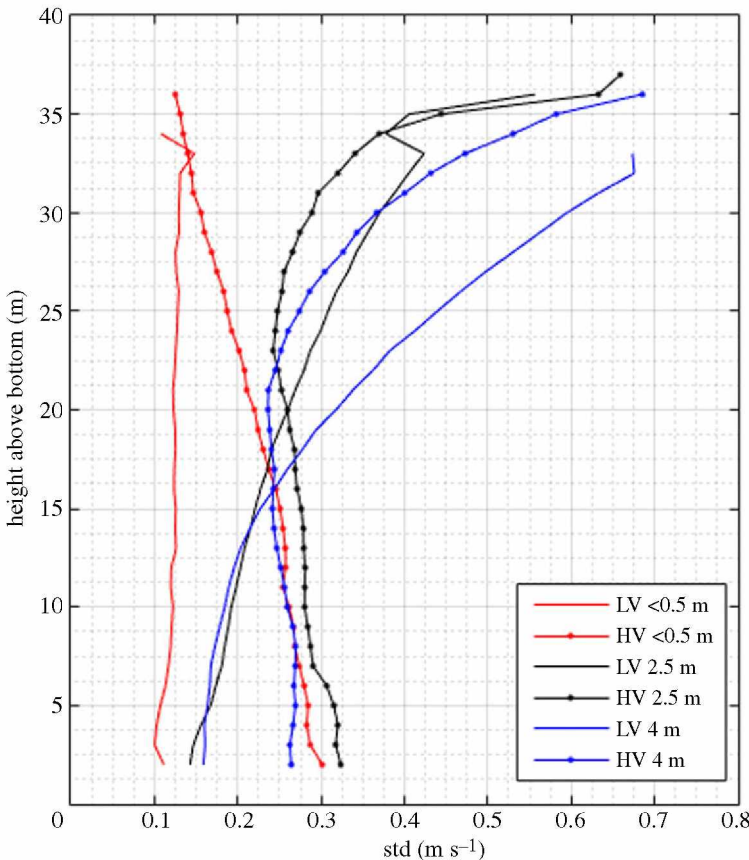


**Figure 9.** Vertical profiles of standard deviation of current velocity from S1-ADCP for three  $H_s$  (less than 0.5, 2.5 and 4 m) and for two flow conditions (low mean velocity,  $LV \sim 0.5 \text{ m s}^{-1}$ , and high mean velocity,  $HV \sim 2.6 \text{ m s}^{-1}$ ). (Online version in colour.)

Another source of HF variability revealed by ADCP measurements is related to a complex wind/wave forcing. Strong variations in meteorological and hydrodynamic conditions make the study of the interaction between tidal currents, waves and wind difficult, as the intensity and direction of waves and wind have to be taken into account.

Two additional situations, corresponding to high waves ( $H_s = 2.5 \text{ m}$  and  $H_s = 4 \text{ m}$ ), were analysed for two flow conditions (mean current speed  $0.5$  and  $2.6 \text{ m s}^{-1}$ ) during flood tide. The preliminary results are shown in figure 9 by blue and black curves. The current direction is northward (flood flow condition) and the waves come almost against the current with an angle less than  $90^\circ$ . The wind speed varies from  $11$  to  $16 \text{ m s}^{-1}$ . In all cases, current speed fluctuations are large in the upper part of the water column as a result of wave-induced orbital motions, then decrease downward under the effect of bottom friction. In the bottom layer, the values of standard deviation of velocity range between  $0.10$  and  $0.16 \text{ m s}^{-1}$  for low velocity and increase up to  $0.3 \text{ m s}^{-1}$  for high velocity.

However, in the upper half of the water column, the level of velocity variability strongly depends on the flow regime. Two distinct situations are identified. For the same sea state, the standard deviation is larger for low current speed (blue and black lines in figure 9) than for high current speed (blue and black points in figure 9). When the waves are almost against the current, the effect of the current seems to reduce wave-related speed fluctuations in the surface layer. This result, previously obtained in numerical simulations by Bennis *et al.* [17], reveals a complex modulation of tidal current speeds by wave forcing.

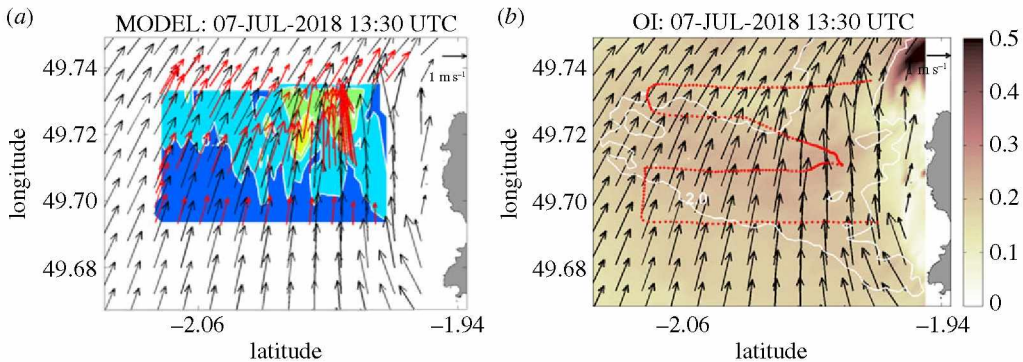


**Figure 10.** (a) Vertically averaged underway velocities (red vectors) obtained during the ADCP survey on July 7, 2018, 11:20–15:40 UTC. Modelled velocity vectors (black) were taken at mid-time of the surveyed period (13:30 UTC) and match peak flood flow. Colour shading shows the difference between the observed velocities and modelled velocities, with contour lines of velocity difference 0.2, 0.4 and 0.5  $\text{m s}^{-1}$  given in white. Modelled velocities, used in comparison, were interpolated in space and time onto measurement points; (b) Optimally interpolated velocity field (black vectors) obtained at mid-time of the ADCP survey: 7-Jul-2018 13:30 UTC. Background shading shows the correction of the modelled velocity field as the result of optimal interpolation of towed ADCP measurements. Red points represent the location of 1 min averaged towed ADCP measurements. The velocity contour 2  $\text{m s}^{-1}$  of the optimally interpolated velocity field is shown in white. (Online version in colour.)

The contribution of wave motions is visible up to a depth of 15 m above the bottom for low flow speed and 20 m above the bottom for high speed. Below this depth, the level of velocity fluctuations is globally similar and depends only on flow conditions. The explanation is simple: the turbulence generated by bottom friction reaches such a high level in the lower layer that additional fluctuations in speed due to waves cannot increase it. Other methods of analysis should be used (e.g. two-dimensional spectral analysis) to separate the contribution of waves to the total variation in current velocity.

### (c) Assessing the spatial variability of currents

Figure 10 shows the flood flow velocity field measured by towed ADCP during neap tide conditions. Velocity profiles from transect surveys were depth averaged and time averaged within 1 min intervals (every fourth velocity vector is shown). Velocities extracted from model post-simulations at mid-time of the ADCP survey are also shown. Both quantities characterize the depth averaged flow and are easy to compare. Visual inspection reveals a good agreement for the direction of the velocity vectors. For detailed assessment of the model skill, we need to take into account the tidal flow evolution during the 4.5 hour survey period. Hence, the model-data misfit was estimated by performing space–time interpolation of model velocities into measurement points. The resulting discrepancy varied between 0.05 and 0.5  $\text{m s}^{-1}$  (figure 10a), with the maximum value achieved in the central sector of the surveyed area where the strongest currents occur. On average, the model was found to underestimate the velocity magnitude by 15%. After performing OI, the overall discrepancy with the model dropped down to 7%. At each time step, the modelled velocities were corrected by observations acquired during the survey. The value of correction varies in space and time and figure 10b shows a typical distribution of this quantity which reaches 0.2  $\text{m s}^{-1}$  in a large central part of the surveyed area during peak flood flow (13:30 UTC). As the result of OI of the towed ADCP measurements, a significant advance in representation of the spatial variability of the tidal circulation in Alderney Race was achieved with much better agreement between the model post-simulations and observations. At the same time, the method provides an indication of the areas where the model has difficulties in reproducing the current velocities accurately. This is another advantage of application of the OI technique.

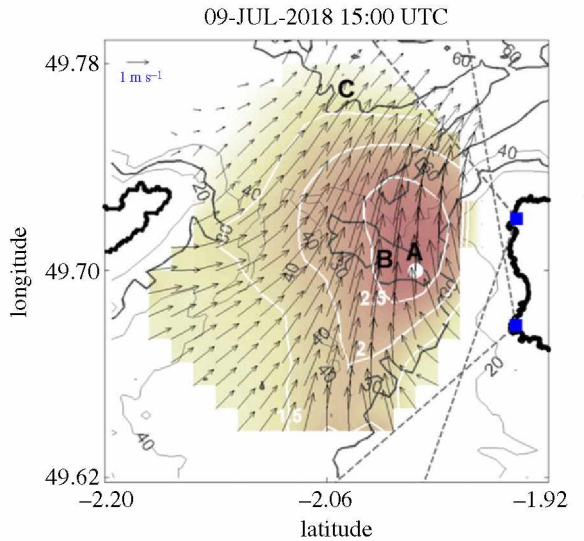


**Figure 11.** Surface current velocities from HF radar measurements during peak flood flow on July 9 2018 15:00 UTC. Colour shading gives the flow speed with velocity contours  $1.5, 2.0, 2.5 \text{ m s}^{-1}$  shown in white. White dot shows the strongest current location. Grey solid lines show the bathymetry contours 20, 30, 40 and 60 m (30 m and 60 m isobaths are highlighted by dark grey). Grey dashed lines show the radar coverage zone. Radar location is given in blue. A, B, C match locations discussed in the text. (Online version in colour.)

Another practical way of assessing the space–time variability of circulation in the Alderney Race is the remote sensing of surface currents by HF radars. We decided to present in this section only one example of the radar-derived velocity field in order to highlight the capabilities of this technique to capture the spatial structure of the flow in detail (for further results the reader is referred to [41]). Figure 11 shows a snapshot of surface current velocities during peak flood flow on July 9, 15:00 UTC. Measurements cover the period of neap tide conditions with moderate wind from the west ( $5 \text{ m s}^{-1}$  wind speed). Due to current convergence observed in the southern sector of the study area, the tidal stream acquires a velocity up to  $2.8 \text{ m s}^{-1}$  (location A) within a broad jet located approximately 5 km offshore with velocities larger than  $2.5 \text{ m s}^{-1}$ . The flow is guided by the bathymetry and large velocity values result from the tidal-stream acceleration over a plateau with depth not exceeding 30 m (location B). The decrease of current speed in the northern sector is also related to bathymetric features, i.e. an abrupt increase of depth to more than 60 m in the vicinity of the La Hague deep (location C). Figure 11 shows that a region with surface flow speeds exceeding  $2 \text{ m s}^{-1}$  spans approximately half of the Race and is located in the East Race—in French territorial waters.

It is interesting to compare the velocity fields acquired by two independent measurement techniques (figures 10b and 11). Both fields correspond to peak flood flow, separated by four tidal cycles under stationary atmospheric conditions. As the result of OI of the towed ADCP measurements, the shape of the area with large velocities (velocity contour  $2 \text{ m s}^{-1}$  in figure 10b) appeared different. Its westward extension became two times larger and the region with flow speeds exceeding  $2 \text{ m s}^{-1}$  matches better the velocity pattern derived from HF radar measurements. Of course, the direct comparison of surface and depth averaged velocities is not relevant (observations are separated by four tidal cycles), but it gives confidence in the results of optimal interpolation.

## 4. Discussion

Tidal-stream energy conversion by in-stream devices is in favour as a renewable energy resource in many European countries. High degree of predictability, close to shore location, and low environmental impacts make this resource attractive. Different technologies are operating today at pilot sites (see [12] for technology description). In order to determine the commercial viability of any project prior to device deployment, to optimize the energy conversion, it is required to properly characterize the environmental conditions at the sites and thus facilitate the process of selecting tidal power devices appropriate for industrial use. Flow characterization for the tidal-stream energy sector also aims to generate input data relevant to engineering models that are used to assess resource availability and to plan on-site activity such as installation and maintenance.

This paper presents an extensive database of oceanographic and meteorological parameters acquired between April 2017 and July 2018 at a potential tidal-stream energy site in the eastern sector of the Alderney Race. A large variety of hydrodynamic conditions were covered by observations continuously performed over more than one year. Currents, waves, turbulence and the interaction between these processes can be used to predict available resource at the site (e.g. [44–46]), to determine power quality fluctuations (e.g. [1,11]) and to assess fatigue and extreme loading on TECs (e.g. [9,47,48]).

Measurements of wind and waves at the site (scanning LIDAR and ADCP data) were validated by comparing them with the data acquired by wave buoys located in the Channel Island region (data from French and the UK network were used). Current velocity data were validated by comparing three bottom-mounted ADCP performing velocity measurements simultaneously at three locations: S1, S2 and S3. Although deployed at the southern limit of the maximum current zone, the acquired data allowed us (i) to study currents, waves and the interaction between these processes, as described in [17]; (ii) to perform a comparison of flow velocities acquired in the Alderney Race by different techniques: the remote sensing of surface velocities by HF radars [40] and towed ADCP measurements [21] and (iii) to improve numerical models for better representing physical processes [17] or assessing the tidal-stream resource variability at larger temporal and spatial scales [49].

Characterization of the spatial variability of tidal stream at prospective tidal energy sites is an important research issue (e.g. [7,20,50]). Current asymmetry is thought to be one of the major metrics considered at the early stage of tidal project planning (e.g. [51]). Tidal current asymmetry in the southern sector of the Race, estimated from S1–S3 ADCP data, revealed a flood-tide dominant regime. Thiébaut *et al.* [6] performed the analysis of ADCP data at location S4 (4 km northward) and demonstrated an ebb-dominated current regime. These results support a general conclusion of Lopez *et al.* [40] based on analysis of the HF radar data, that tidal current asymmetry varies spatially at short spatial scales.

Spatial variability of tidal stream was also assessed using towed ADCP measurements. Velocity data from transect surveys offer an excellent opportunity for three-dimensional representation of the velocity field, for improvement of the results of model post-simulations and resource estimation. In a recent study, Thiébaut *et al.* [21] merged the towed ADCP data, acquired during the first survey in the Alderney Race in May 2017 with the model results and obtained a significant change in the spatial pattern of power density distribution at the site. Therefore, a combination of high-resolution modelling and ongoing velocity measurements can provide a more accurate estimation of the spatial and temporal variability of the tidal-stream resource.

Assessment of wind, wave and current velocity time series showed that there are relatively few periods of time characterized by calm weather conditions and sea state ( $H_s < 0.5\text{ m}$  and wind speed  $< 4\text{ m s}^{-1}$ ). Even if they represent only 6% of the whole duration of observations, the data acquired during these periods allow us to assess the interaction between tide currents with bottom topography without wave.

We demonstrated that while the current velocities increase, the TKE and the standard deviation of velocities also increase, with larger values found near the bottom and smaller values near the surface, which is in close agreement with Neill *et al.*, [50] and Tognetti *et al.*, [5]. On the other

hand, the TKE is higher during the ebb tide, while the current speeds are larger during the flood tide. A possible explanation of this difference in ambient level of turbulence can be related to the advection of turbulence by the current (advection term in turbulent energy equation). We assume that the turbulence energy production occurs upstream of the ADCP location (over a shallow water plateau shown by B in figure 11) and this turbulence is advected southward as frozen turbulence. A large asymmetry of TKE at the measurement site and presumable large contribution of TKE advection is an important result of the data analysis. This result highlights the role of the seafloor topography that generates turbulence in the bottom boundary layer. Thiébaut *et al.*, (cf this Theme Issue) who investigated the turbulent energy budget using ADCP data deployed in more energetic sector of the Race (location S4 in figure 1), came to similar conclusions.

As the majority of TECs are designed to be located in the bottom boundary layer, where the flow experiences friction from the seabed, the knowledge of vertical shear of current velocity and the level of ambient turbulence are the major considerations. It is assumed to have important implications for turbine efficiency and resilience (e.g. [48,52]) as well as for the instantaneous power availability, as described in [1,45]. For this reason, TEC developers are particularly interested in detailed characterization of the flow speed and velocity profile shape in the bottom boundary layer. But these two quantities vary considerably in space and time. The magnitude of instantaneous fluctuations can be quantified using velocity time series (cf. Figure 7b). Our analysis revealed a velocity variation of  $1.35 \text{ m s}^{-1}$  in 3 s at 2 and 5 m above the bottom. The time interval corresponds to one revolution of blades of a TEC operating at rotation speed 20 rpm. This example shows how large a variation of loadings on the turbine blades could be.

Studies by Bennis *et al.* [17] and Lewis *et al.* [53] highlighted a large effect of waves on the mean tidal current velocities and also on velocity fluctuations. Low duration of calm periods (6% of the whole period of observation) indicates that the Alderney Race is nearly continuously exposed to large swells and strong winds. This strongly supports the need for studies of waves, wind and tidal current interactions with tidal turbines (e.g. [47]). The wave-current interaction was analysed for two meteorological events with large  $H_s$ : 2.5 and 4 m. The effect of waves on the current was observed in the upper half of the water column extending up to 15 m above the bottom (in these two cases), while turbulent fluctuations of velocity generated by bottom friction appeared dominant in the bottom boundary layer, occupying the lower half of the water column. This may explain an attenuation of the wave effect on current from the mid-depth. Other situations, characterized by wave propagation direction less than  $90^\circ$  with respect to the current direction, were investigated by Bennis *et al.* [17] using numerical modelling. The authors largely used measurements from the database.

## 5. Conclusion

An extensively validated and comprehensive database is an excellent tool to study the hydrodynamic processes and resource distribution at the site. A wide variability of local hydrodynamics, largely affected by swell and strong wind, was observed and characterized. Relatively few periods of time (only 6%) were characterized by calm weather conditions and sea state ( $H_s < 0.5 \text{ m}$  and wind speed  $< 4 \text{ m s}^{-1}$ ). The data acquired during these periods allowed assessment of the interaction of tidal currents with bottom topography. Large velocity fluctuations were observed in the lower half of the water column. The magnitude of fluctuations reached  $1.35 \text{ m s}^{-1}$  in 3 s at 2 and 5 m above the bottom. An asymmetry of TKE between ebb and flood tide was also revealed with a presumable large contribution of advection term in TKE budget. During extreme events, significant wave height,  $H_s$ , reached the maximum value of 8 m, whereas the wind speed exceeded  $20 \text{ m s}^{-1}$ . For moderate and strong sea state conditions ( $H_s = 2.5$  and 4 m), our results revealed a large effect of waves on the current in the upper half of the water column extending up to 15 m above the bottom. Predominant wind and wave direction relative to the flow impacts the waveheight and increases significantly the turbulence kinetic energy of the flow. The instantaneous velocity in the upper layer reached  $7 \text{ m s}^{-1}$ , while turbulent fluctuations of velocity, generated by bottom friction, appeared dominant in the bottom boundary layer.

Spatial variability of the tidal stream was assessed by using towed ADCP and HF radar measurements. It was demonstrated that a combination of high-resolution modelling and ongoing velocity measurements can provide a more accurate estimation of the spatial variability of the tidal stream.

The database could be used for a comprehensive analysis of physical processes governing the flow variability, such as wave-current and wind-current interactions, turbulence and extreme conditions. It could be useful for TEC developers, particularly interested in detailed characterization of the flow conditions and velocity profile shape in the bottom layer. We hope that the results of database analysis represent a significant advance in environmental conditions characterization and provide advanced information to turbine developers.

**Data accessibility.** The data will be accessible for April 2020. All the data acquired in the project will be available to the reader from July 2020 onwards. This data will be available via: <http://www.geoceano.fr/programmes/anr-hyd2m>.

**Authors' contributions.** All of the authors were involved in field campaigns, data processing or data analysis and then writing the paper or proofreading in-depth.

**Competing interests.** We have no competing interests.

**Funding.** Authors are supported by the HYD2M project (ANR-10-IEED-0006-07) funded by the program called 'Investissements d'avenir' for the building of France Energies Marines and the department council of Manche.

**Acknowledgments.** This work benefitted from the funding support from France Energies Marines and the French Government, operated by the National Research Agency under the Investments for the Future program: Reference ANR-10-IEED-0006-07. The study represents a contribution to the project HYD2M of the above program. We would like to acknowledge the crew of the R/V 'Côtes de la Manche'.

## References

- Lewis M *et al.* 2019 Power variability of tidal-stream energy and implications for electricity supply. *Energy*. **183**, 1061–1074. (doi:10.1016/j.energy.2019.06.181)
- Cameron G. (2017-02-21). Atlantis shows turn of speed installing new tidal turbine. The Times. See <https://tethys.pnnl.gov/project-sites/sabella-d10-tidal-turbine-ushant-island>.
- Integrated Ocean Observing System. 2019 Manual for Real-Time Quality Control of In-Situ Current Observations. Technical Report. See <https://ioos.noaa.gov/ioos-in-action/currents/>
- Guerra M, Thomson J. 2017 Turbulence measurements from five-beam Acoustic Doppler Current Profilers. *Am. Meteorol. Soc.* **34**, 1267–1284. (doi: 10.1175/JTECH-D-16-0148.1)
- Tognetti M, Jones D, Neill SP, Lewis M, Ward SL, Piano M, Masters I. 2017 Comparison of 4- and 5 beam acoustic Doppler current profiler configurations for measurement of turbulent kinetic energy. *Energy Procedia*. **125**, 260–267. (doi:10.1016/j.egypro.2017.08.170)
- Thiébaut M, Filipot JF, Maisondieu C, Damblans G, Duarte R, Droniou E, Chaplain N, Guillou S. 2019a A comprehensive assessment of turbulence at a tidal-stream energy site influenced by wind-generated ocean waves. *Energy*. **191**, 116550. (doi:10.1016/j.energy.2019.116550)
- Thiébaut M, Sentchev A. 2017 Asymmetry of tidal currents off the W. Brittany coast and assessment of tidal energy resource around the Ushant Island. *Renew. Energy*. **105**, 735–747. (doi:10.1016/j.renene.2016.12.082)
- Gooch S, Thomson J, Polagye B, Meggitt D. 2009 Site characterisation for tidal power. In OCEANS 2009, MTS/IEEE Biloxi-Marine Technology for our future: global and local challenges, pp. 1–10.
- Milne, IA, Day, AH, Sharma, RN, Flay RGJ. 2015 Blade loading on tidal turbines for uniform unsteady flow. *Renew. Energy*. **77**, 338–350. (doi:10.1016/j.renene.2014.12.028)
- Blackmore T, Myers LE, Bahaj AS. 2016 Effects of turbulence on tidal turbines: Implications to performance, blade loads, and condition monitoring. *Int. J. Mar. Energy*. **14**, 1–26. (doi:10.1016/j.ijome.2016.04.017)
- Sentchev A, Thiébaut M, Schmitt FG. 2020 Impact of turbulence on power production by a free-stream tidal turbine in real sea conditions. *Renew. Energy*. **147**, 1932–1940. (doi:10.1016/j.renene.2019.09.136)
- Dorward M, Sellar B, Old C, Thies PR. 2019 Currents, Waves and Turbulence Measurement: A View from Multiple Industrial-Academic Projects in Tidal Stream Energy. In *IEEE/OES twelfth current, waves and turbulence measurement (CWTM)*, pp. 1–10.

13. Coles DS, Blunden LS, Bahaj AS. 2017 Assessment of the energy extraction potential at tidal sites around the Channel Islands. *Energy*. **124**, 171–186. (doi:10.1016/j.energy.2017.02.023)
14. Draper S, Adcock TAA, Borthwick AGL, Houlsby AT. 2014 Estimate of the tidal stream power resource of the Pentland Firth. *Renew. Energy* **63**, 650–657. (doi:10.1016/j.renene.2013.10.015)
15. Furgerot L, Poprawski Y, Violet M, Poizot E, Bailly du Bois P, Morillon M, Méar Y. 2019 Mobile vs. encrusted quaternary sediments and their bedrock in a tide-dominated environment (Alderney Race). *J. of Maps*. **15**, 708–718. (doi:10.1080/17445647.2019.1657510)
16. Mercier P, Grondeau M, Guillou S, Thiébot J, Poizot E. 2020 Numerical study of the turbulent eddies generated by the seabed roughness. Case study at a tidal power site. *Appl. Ocean Res.* **97**, 102082. (doi:10.1016/j.apor.2020.102082)
17. Bennis A-C, Furgerot L, Bailly Du Bois P, Dumas F, Odaka T, Lathuilière C, Filipot J-F. 2020 Numerical modelling of three-dimensional wave-current interactions in complex environment: application to Alderney Race. *Appl. Ocean Res.* **95**, 102021. (doi:10.1016/j.apor.2019.102021)
18. Thiébot J, Bailly du Bois P, Guillou S. 2015 Numerical modeling of the effect of tidal stream turbines on the hydrodynamics and the sediment transport – Application to the Alderney Race (Raz Blanchard), France. *Renew. Energy* **75**, 356–365. (doi:10.1016/j.renene.2014.10.021)
19. Goddijn-Murphy L, Woolf DK, Easton MC. 2013 Current patterns in the inner sound (Pentland Firth) from underway ADCP data. *J. Atmos. Ocean. Technol.* **30**, 96–111. (doi:10.1175/JTECH-D-11-00223.1)
20. Thiébaut M, Sentchev A. 2016 Tidal stream resource assessment in the Dover Strait (eastern English Channel). *Int. J. Mar. Energy*. **16**, 262–278. (doi:10.1016/j.ijome.2016.08.004)
21. Thiébaut M, Sentchev A, Bailly du Bois P. 2019b Merging velocity measurements and modeling to improve understanding of tidal stream resource in Alderney Race. *Energy*. **178**, 460–470 (doi:10.1016/j.energy.2019.04.171)
22. Bailly du Bois P, Dumas F, Morillon M, Furgerot L, Voiseux C, Poizot E, Méar Y, Bennis A-C. 2020 The Alderney Race: general hydrodynamic and particular features. *Phil. Trans. R. Soc. A* **378**, 20190492. (doi:10.1098/rsta.2019.0492)
23. Bailly du Bois P, Dumas F, Solier L, Voiseux C. 2012 In situ database toolbox for short-term dispersion model validation in macro-tidal seas, application for 2D-model. *Cont. Shelf Res.* **36**, 63–82. (doi:10.1016/j.csr.2012.01.011)
24. Kirincich AR, Rosman JH. 2011 A comparison of methods for estimating Reynolds stress from ADCP measurements in wavy environments. *Am. Meteorol. Soc.* **28**, 1539–1553. (doi:10.1175/JTECH-D-11-00001.1)
25. Goring D, Nikora V. 2002 Despiking Acoustic Doppler Velocimeter Data. *J. hydraul. eng.* **128**, 117–126. (doi:10.1061/(ASCE)0733-9429(2002)128:1(117))
26. Teledyne RD Instruments. 2007. Workhorse technical manual. 198pp.
27. Milne IA, Sharma RN, Flay RGJ, Bickerton S. 2013 Characteristics of the turbulence in the flow at a tidal stream power site. *Phil. Trans. R. Soc. A* **371**, 20120196. (doi:10.1098/rsta.2012.019)
28. Teledyne RD Instruments. 2011. WavesMon v3.08 – User’s Guide. 72p.
29. Wiberg PL, Sherwood CR. 2008 Calculating wave-generated bottom orbital velocities from surface-wave parameters. *Comput. Geosci.* **34**, 1243–1262. (doi:10.1016/j.cageo.2008.02.010)
30. Bailly du Bois P, Pouderoux B, Dumas F. 2014 System for high-frequency simultaneous water sampling at several depths during sailing. *Ocean Engineering* **91**, 281–289. (doi:10.1016/j.oceaneng.2014.09.022)
31. Vennell R. 2006 ADCP measurements of momentum balance and dynamic topography in a constricted tidal channel. *J. Phys. Oceanogr.* **36**, 177–188. (doi:10.1175/JPO2836.1)
32. Gandin L. 1963 Objective analysis of meteorological fields, Gidrometeorologicheskoe stol'stvo, Leningrad, translated from Russian, Israel Program for Scientific Translation, Jerusalem. *Q. J. R. Meteorol. Soc.* **92**, 447.
33. Thiébaux H, Pedder M, 1987. *Spatial objective analysis with applications in atmospheric science*. London, UK: Academic Press.
34. Wunsch C. 1996 The Ocean Circulation Inverse Problem. Cambridge, UK: Cambridge University Press.
35. Sentchev A, Yaremchuk M. 2016 Monitoring tidal currents with a towed ADCP system. *Ocean Dyn.* **66**, 119–132. (doi:10.1007/s10236-015-0913-z)

36. Stewart RH, Joy JW. 1974 HF radio measurements of surface currents. *Deep Sea Res. Oceanogr. Abstracts.* **21**, 1039–1049. (doi:10.1016/0011-7471(74)90066-7)
37. Gurgel KW, Essen HH, Kingsley SP. 1999 High-frequency radars: physical limitations and recent developments. *Coastal Eng.* **37**, 201–218.
38. Schmidt RO. 1986 Multiple emitter location and signal parameter estimation. *Antennas Propag. IEEE Trans.* **34**, 276–280. (doi:10.1109/TAP.1986.1143830)
39. Lipa B, Nyden B, Ullman DS, Terril E. 2006 SeaSonde radial velocities: derivation and internal consistency. *IEEE J. Oceanic Eng.* **31**, 850–861. (doi:10.1109/JOE.2006.886104)
40. Lopez G, Bennis, A-C, Barbin Y, Benoît L, Cambra R, Sentchev A. 2019 Surface hydrodynamics of the Alderney Race from HF radar measurements. In *Proceeding of the 13th European wave and tidal energy conference, Naples, Italy, 3–6 September 2019*, pp. 1–10. EWTEC.
41. Lopez G, Bennis A-C, Barbin Y, Sentchev A, Benoit L, Marié L. 2020 Surface currents in the Alderney Race from high-frequency radar measurements and three-dimensional modelling. *Phil. Trans. R. Soc. A* **378**, 20190494. (doi:10.1098/rsta.2019.0494)
42. Yaremchuk M, Sentchev A. 2009 Mapping radar-derived sea surface currents with a variational method. *Cont. Shelf Res.* **29**, 1711–1722. (doi:10.1016/j.csr.2009.05.016)
43. Archer A. 2013 World's highest tides: Hypertidal coastal systems in North America, South America and Europe. *Sediment. Geol.* **284**, 1–25. (doi:10.1016/j.sedgeo.2012.12.007)
44. Guillou N, Chapalain G, Neill SP. 2016 The influence of waves on the tidal kinetic energy resource at a tidal stream energy site. *Appl. Energy.* **180**, 402–415. (doi:10.1016/j.apenergy.2016.07.070)
45. Lewis SP, Neill MR, Hashemi MR, Reza M. 2014 Realistic wave conditions and their influence on quantifying the tidal stream energy resource. *Appl. Energy.* **136**, 495–508.
46. Hashemi MR, Neill SP, Robins PE, Davies AG, Lewis MJ. 2015 Effect of waves on the tidal energy resource at a planned tidal stream array. *Renew. Energy.* **75**, 626–639. (doi:10.1016/j.renene.2014.10.029)
47. Tatum SC, Frost CH, Allmark M, O'Doherty DM, Mason-Jones A, Prickett PW, Grosvenor RI, Byrne CB, O'Doherty T. 2016 Wave-current interaction effects on tidal stream turbine performance and loading characteristics. *Int. J. Mar. Energy.* **14**, 161–179. (doi:10.1016/j.ijome.2015.09.002)
48. Liu P, Veitch B. 2012 Design and optimization for strength and integrity of tidal turbine rotor blades. *Energy* **46**, 393–404. (10.1016/j.energy.2012.08.011)
49. Thiébot J, Guillou S, Droniou E. 2020 Influence of the 18.6-year lunar nodal cycle on the tidal resource of the Alderney Race, France. *Appl. Ocean Res.* **97**, 102107. (doi:10.1016/j.apor.2020.102107)
50. Neill SP, Hashemi MR, Lewis MJ. 2014 The role of tidal asymmetry in characterizing the tidal energy resource of Orkney. *Renew. Energy.* **68**, 337–350. (doi:10.1016/j.renene.2014.01.052)
51. Polagye B, Thomson J. 2013 Tidal energy resource characterization: Methodology and field study in Admiralty Inlet, Puget Sound, WA (USA). *Proc. Inst. Mech. Eng. A J. Power Energy.* **227**, 352–367. (doi:10.1177/0957650912470081)
52. Milne IA, Day AH, Sharma RN, Flay RGJ. 2016 The characterisation of the hydrodynamic loads on tidal turbines due to turbulence. *Renew. Sustain. Energy Rev.* **56**, 851–864.
53. Lewis M, Neill S, Robins P, Hashemi M, Ward S. 2017 Characteristics of the velocity profile at tidal-stream energy sites. *Renew. Energy.* **114**, 1–15. (doi:10.1016/j.renene.2017.03.096)